RESEARCH PAPER

Hydrocarbon potentialities of carbonate rocks for Abu Roash/D Member: Petrosannan field, Abu Sannan area North Western Desert, Egypt

Aly El-Shaer [a,*], Mohamed A. Kassab [b], Amin E. Khalil [c], Nouran S. Salama [c]

[a] Petrosannan Petroleum Company, Cairo, Egypt
[b] Egyptian Petroleum Research Institute, 11727, Cairo, Egypt
[c] Department of Geology, Helwan University, Cairo, Egypt

Abstract

This study aims to examine the hydrocarbon potential of Abu Roash/D member (AR/D) in the Petrosannan field. The Petrosannan Field's primary hydrocarbon production comes from siliciclastic reservoirs, particularly the Abu Roash/C, E, and G members. Despite promising characteristics displayed by AR/D, early exploration efforts involved a single drill stem test (DST) conducted for one well in a cased-hole environment, yielding no data and resulting in an incomplete assessment of the reservoir's production potential. This paper presents an integrated analysis of conventional logs, X-tended Range Micro Imager (XRMI), and core data from five wells (A, B, C, D, and E), employing Techlog and Petrel software. Petrophysical analysis reveals porosity ranging from 13 to 15% and water saturation between 35 and 70%, with X-tended Range Micro Imager data detecting distinct patterns within partially open fractures, suggesting potential improvements in permeability. Petrographic analysis of core samples unveils an average porosity of ~16%, with X-ray diffraction (XRD) analysis confirming calcite as the dominant mineral, constituting 95.9% of the composition. Despite the high porosity observed, AR/D faces challenges associated with reservoir tightness and developmental complexities. This research aims to address these challenges and bridge existing knowledge gaps. Based on the acquired data and understanding of reservoir characteristics, the study hypothesizes that stimulation techniques, such as acid treatment or hydraulic fracturing, could mitigate reservoir tightness and enhance overall hydrocarbon recovery. Subsequent field tests involving hydraulic fracturing in a suitable well yielded an average production rate of 100 barrels of oil per day, underscoring the hydrocarbon potential of AR/D carbonate in the Petrosannan field. This study offers valuable insights for unlocking the potential of carbonate reservoirs in the region, thus contributing to global energy security.

Keywords: Carbonate reservoirs, Heterogeneity, Hydrocarbon potential, Petrographic analysis, Stimulation techniques

1. Introduction

The Petrosannan field, encompassing 114 km^2 in Egypt's northwestern desert, situated between latitudes 29° 28′ N and 29° 43′ N, and longitudes 28° 18′ E and 28° 28′ 30″ E (Fig. 1). The northern portion of the Western Desert has a rich stratigraphy due to the presence of a broad sedimentary sequence that runs from the early era to the present. This stratigraphic richness offers unique insights into the geological history of the area, including information about former habitats, temperature changes, and the evolution of living forms (Fig. 2).

Petrosannan field is situated in the south-central part of the Abu El Gharadig basin (AG). Abu Roash/D member (AR/D) is indeed recognized as a significant hydrocarbon producer within the AG basin,[1,2] which is renowned for its petroleum production in the Western Desert region. The thickness of AR/D in the vicinity of the study ranges from 80 to 100 m; it predominantly consists of limestone with occasional interspersed thin shale layers.[3]

Received 26 March 2024; revised 27 May 2024; accepted 11 June 2024.
Available online 30 July 2024

* Corresponding author. First Settlement Services Area, New Cairo, 13211, Egypt.
E-mail address: geo.elshaer@gmail.com (A. El-Shaer).

https://doi.org/10.62593/2090-2468.1037

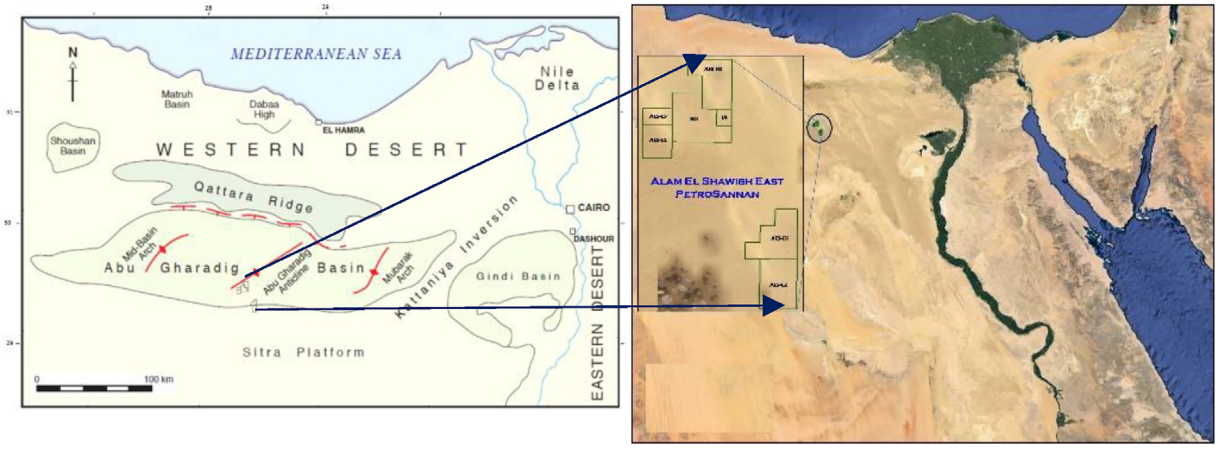

Fig. 1. The study area location map.

The AG basin is a significant geological feature in the Western Desert district, covering approximately 3.6% of its area. It is characterized by its oblique rift structure, stretching about 300 km in length and 60 km in width,[4,5] Its origin was initially believed to be a series of pull-apart basins, likely formed through Earth's crust extension due to tectonic forces.[6] During the Cretaceous period, which is a geological epoch spanning from ~145 to 66 million years ago, the main faults inside the AG basin are oriented in a WNW-ESE direction, while the adjacent fault from northward has a common E-W direction, which obviously implies the influence of pre-existing E-W faults on the overall direction of the basin.[4,7] It is an extended depression spreading along the Qattara Depression from the westward and the Kattaniya Horst from the eastward. The basin is bordered by double basement uplifts, which are the Sharib-Sheiba-Rabat platform to the north and the Cairo-Bahariya uplift to the south.[8]

The Petrosannan field's primary hydrocarbon production comes from siliciclastic reservoirs, particularly the Abu Roash/C, E, and G members, and the Bahariya formation. However, for carbonate reservoirs, such as AR/D, a drill stem test was applied to just one well in a cased-hole environment without any stimulation program. Unfortunately, the drill stem test yielded no data, leading to an incomplete evaluation of the reservoir's production potential.

Carbonate reservoirs hold immense potential for meeting future global energy demands, as evidenced by published literature, which indicates that they harbor approximately 60% of the world's oil reserves.[9,28]

Exploration and development of carbonate reservoirs present greater challenges compared with their siliciclastic counterparts. This complexity arises from inherent heterogeneities in these reservoirs, encompassing variations in lithology, mineralogy, pore types, connectivity, and textures. Consequently, a substantial portion of carbonate reservoirs remain nonproducing or are exploited at sub-commercial rates.[10] For carbonate reservoirs, there is no quantitative way to determine if hydraulic fracturing or acid fracturing is the proper strategy for well stimulation.[11] Well stimulation technique has been demonstrated to be effective in boosting hydrocarbon recovery through creating a conductive fracture and improving well productivity in tight and extremely low-permeable reservoirs.[12]

The study intends to examine the hydrocarbon potential of AR/D carbonate in Petrosannan field by a comprehensive workflow for getting a better understanding of the characteristics of carbonate reservoirs, which will help operating companies efficiently control the production from carbonate reservoirs and deplete a hydrocarbon resource in a profitable way.

The analysis revealed that AR/D is primarily composed of limestone, exhibiting porosity between 13 and 15% and water saturation ranges from 35 to 70%. Moreover, the interpretation of X-tended Range Micro Imager (XRMI) data suggests the presence of partially open fractures, potentially enhancing permeability. Core analysis confirmed the porous nature of the rock, with an average porosity of 15%, radiography diffraction (XRD) analysis indicated a dominance of calcite, accounting for approximately 95.9% of the mineral composition.

Based on the obtained data and understanding of the reservoir characteristics, the study hypothesizes that the application of stimulation techniques, such as acid treatment or hydraulic fracturing, could potentially accelerate production and improve the overall hydrocarbon recovery from the AR/D. One

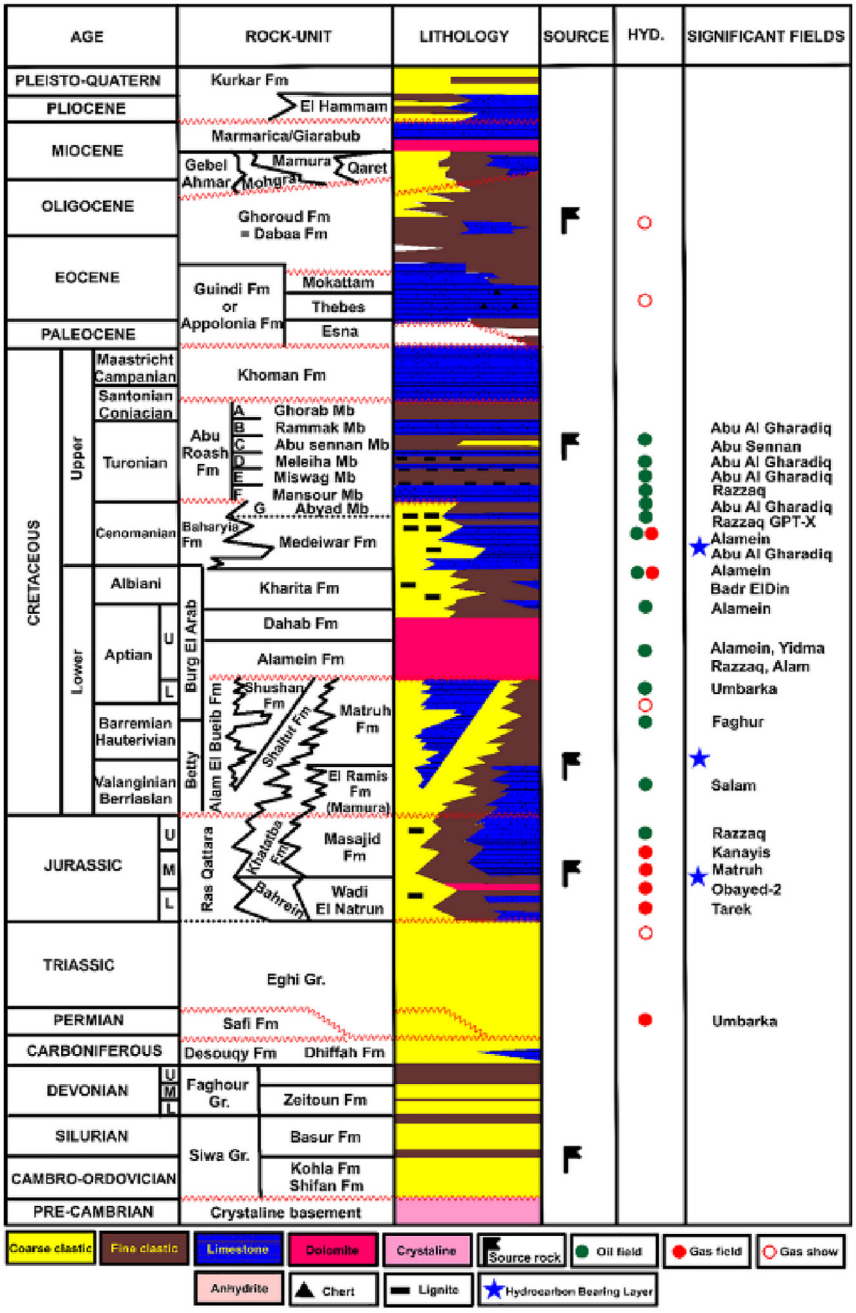

Fig. 2. Generalized Lithostratigraphic column of Western Desert, after.

of the candidate wells exhibiting favorable reservoir parameters was tested. The well has demonstrated an average daily oil production of ~100 barrels.

2. Methods and techniques

The integration of traditional well logs, advanced imaging techniques as XRMI, and core data enables a more robust characterization of subsurface reservoirs.

Corrections were applied before performing calculations to mitigate the influence of various parameters on the well-log data, such as lithology, mud weight, borehole conditions, and formation temperature. The petrophysical characteristics of the intervals of interest were determined using the adjusted data.

2.1. Identification of lithology

Lithology determination, crucial for reservoir characterization, is addressed using well logs

primarily influenced by rock characteristics, such as gamma-ray (GR) logs and neutron-density (DEN) cross-plots.[13] GR logs detect the natural radioactivity emitted by rocks, which might change based on their composition. A baseline of 20 API is used to differentiate between clastic and nonclastic rocks. Values below 20 API are characterized as nonclastic lithology (carbonate rocks), while values greater than 20 API are classified as clastic lithology.[14]

The neutron-density cross-plot is an approach used for the lithological identification and characterization of formations. It includes graphing neutron porosity against bulk density. Each rock type has a unique position on the plot due to their differing compositions.[14]

2.2. Volume of shale (Vsh)

Shale volume (Vsh) is a critical parameter in reservoir evaluation, impacting porosity, permeability, and hydrocarbon potential. GR logs offer a valuable tool for Vsh determination due to their sensitivity to the naturally occurring radioactive elements concentrated in shales. The procedure of calculating Vsh begins with Equation (1).[14]

$$I_{GR} = \frac{GR_{log} - GR_{min}}{GR_{max} - GR_{min}} \tag{1}$$

GR_{min} is GR matrix. GR_{max} is GR shale (clay zone). I_{GR} represents the index values and GR_{log} represents reading for the zones.

Building upon this, Equations (2) and (3) provide specific formulas for calculating Vsh tailored for different lithologies: Equation (2) for consolidated earlier rocks (Paleozoic and Mesozoic) and Equation (3) for younger, unconsolidated rocks (Tertiary).[15]

$$\mathrm{Vsh} = 0.33[2(2{*}\mathrm{IGR}) - 1] \tag{2}$$

$$\mathrm{Vsh} = 0.083[2(3.7{*}\mathrm{IGR}) - 1] \tag{3}$$

After computing the Vsh value, it must be corrected before estimating the porosity.[16]

2.3. Porosity (Ø)

The density-neutron logs are useful records to determine rock porosity. The tool response for these devices is influenced by the formation of porosity, fluid, and matrix.[17]

$$\varnothing_D = \frac{\rho_{ma} - \rho_b}{\rho_{ma} - \rho_f} - V_{sh}\frac{\rho_{ma} - \rho_{sh}}{\rho_{ma} - \rho_f} \tag{4}$$

Where ρ_{ma} is the density of the matrix ρ_b signifies the density log reading for the formation and ρ_f is the density of the fluid.

The equations (5) and (4) are used for obtaining the corrected neutron porosity and the corrected density porosity.[18]

$$\varnothing_{Ncorrected} = \varnothing_N - \left[\left(\frac{\varnothing_{Nclay}}{0.45}\right) \times 0.30 \times Vsh\right] \tag{5}$$

$$\varnothing_{Dcorrected} = \varnothing_N - \left[\left(\frac{\varnothing_{Dclay}}{0.45}\right) \times 0.13 \times \mathrm{Vsh}\right] \tag{6}$$

The equation (7) is used for finding the corrected porosity values.[14]

$$\varnothing corr = \sqrt{\frac{\varnothing_{Ncorrected}{}^2 + \varnothing_{Dcorrected}{}^2}{2}} \tag{7}$$

$\varnothing_{Dcorrected}$ is the estimated corrected density and $\varnothing_{Ncorrected}$ is the estimated corrected porosity. From the equation (8) the effective porosity value ($\varnothing_{Eff}$) can be calculated.[19]

$$\varnothing_{Eff} = \varnothing corr{*}(1 - V_{sh}) \tag{8}$$

2.4. Water saturation (SW)

The following formula proposed the relationship between water saturation, rock resistivity, formation factor, and water resistivity in the formation illustrated in equation (9).[20]

$$S_w = \left(\frac{a \times R_w}{\varnothing^m \times R_t}\right)^{\frac{1}{n}} \tag{9}$$

Where ∅ is the formation porosity, (a) represents tortuosity, (m) represents cementation factor, (n) represents saturation exponent, (Rw) represents water resistivity of the formation, (Rt) represents resistivity of the formation and (Sw) represents saturation of the water. The following are the assumed values for (RW = 0.065 Ω m, a = 1, m = 1.8 and n = 2).

From SW data, the equation (10) can be applied to calculate hydrocarbon saturations (Sh).[21]

$$S_h = 1 - S_w \tag{10}$$

2.5. XRMI data

The XRMI tool has been designed to provide high-quality images even in settings if the mud resistivity to formation resistivity percentage (Rt:Rm) becomes greater.[22] The XRMI equipment produces

high-quality borehole images using pads mounted on six articulated arms with a high sampling rate (120 samples per foot). A high resistivity zone is shown by a light-shaded area on the XRMI log, and a low resistivity zone is indicated by a dark-shaded area. Following processing of the XRMI data, interpretation is carried out to define all the rock features surrounding the drilled well such as sedimentary structures, channels, vugs, and fractures.

2.6. Petrographical and XRD analysis

Petrographic and mineralogical analyses were conducted on core samples to characterize their reservoir quality. These analyses included:

Thin-section examination: 10 carbonate core samples were analyzed for texture, composition, porosity, classification, and diagenetic history. Blue-tinted resin aided in porosity observation.

SEM analysis: Four core samples were analyzed using SEM to understand their microstructure, mineralogy, and other features at high magnification.

XRD analysis: Three core samples were analyzed using XRD to determine their semi-quantitative mineralogical composition. Samples were micronized before analysis.

3. Results and discussion

3.1. Petrophysical examination

Figures 3–7 present a comprehensive array of logging parameters meticulously organized across tracks, offering significant insights into the reservoir characteristics of the zone of interest. These parameters encompass critical aspects such as Formation Top in track one, measured depth (MD) in track two, true vertical depth subsea (TVDss), GR log in track three, Resistivity logs in track four (RES DEP, RES SLW, MSFL), Photoelectric log (PE), formation density log (DEN), density correction log (DENC) and Neutron porosity log (NEU) in track five, total gas reading in track six, Vsh in track seven, total porosity in track eight, water saturation in track nine, and lithology in track 10 and formation name in track 11.

This comprehensive evaluation focused meticulously on key parameters such as lithology determination, Vsh, porosity, and water saturation, providing a robust petrophysical interpretation of the AR/D reservoir in the study area, with indications of the reservoir's AR/D potential.

The reservoir's lithology may be discovered by utilizing a combination of all achievable logs, such as neutron, GR, density and photoelectric logs.[19,23] By combining information from the GR log (Track three) and the density-neutron cross-plot (Fig. 8), Analysis indicates that the predominant lithology of the reservoir is limestone. Fig. 8 presents a cluster towards lower density values, suggesting a potential dual influence: fracturing within the limestone and also due to reservoir gas bearing effect gas.

The calculated Vsh (Track seven) was very low, ranging from 0.005 to 0.014. This low shale influence, a positive indicator for reservoir quality, suggests good potential for efficient fluid flow within the zone of interest. The log response represents the range of the estimated porosity values ranging from 13% to 15% (Track eight), alongside a notable variation in estimated water saturation within the reservoir, ranging from 0.35 to 70% (Track nine). Although direct measurements of hydrocarbon saturation were unavailable, estimation is inferred by subtracting the calculated water saturation from 100% (total saturation).

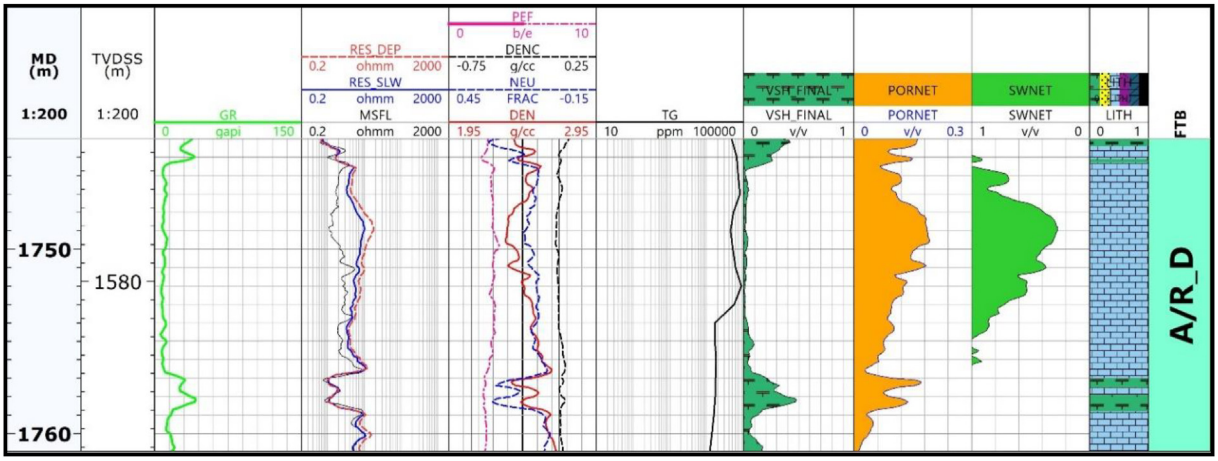

Fig. 3. Vertical distribution results of petrophysical and Lithology of AR/D reservoir in A well.

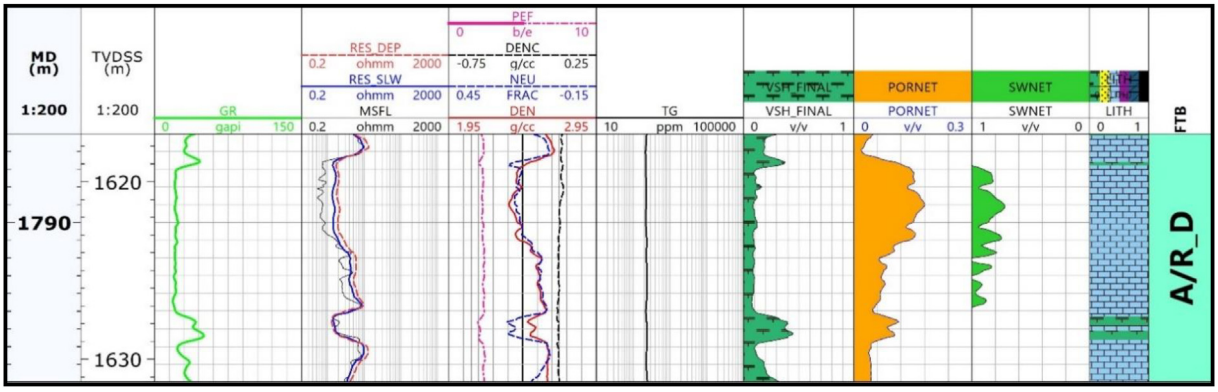

Fig. 4. Vertical distribution results of petrophysical and Lithology of AR/D reservoir in B well.

3.2. XRMI data

The ultimate purpose of this tool is to provide a complete understanding of the primary structural features impacting the expected hydrocarbon zone of the AR/D carbonate. The manual picking and interpretation of the XRMI image demonstrate that drilling constructed induced fractures within the AR/D interest zone, as well as interpreted partial open fractures with diverse directions, which may improve permeability and contribute to HC production (Fig. 9).

3.3. Petrographical and XRD analysis

Thin-section analysis revealed the presence of bioclasts (foraminiferal tests) within a micritic matrix with traces of pyrite (Fig. 10). The identified pore types include intercrystalline, channel, and intragranular pores, characterized by generally low interconnectivity (Figs. 10 and 11). The diagenetic processes perform an essential role in the evolution of carbonate rocks, influencing their porosity, permeability, and overall reservoir quality in the subsurface.[24] The early diagenetic history of carbonates is characterized by various processes, including pore filling, grain replacement, carbonate cementation (mainly calcite), and matrix micritization.[25,26] Diagenetic processes, such as pore filling, grain replacement, and micritization, were observed (Figs. 11 and 12). The carbonate rocks can be classified into four main depositional textures (Mudstone, Wackestone, Packstone, and Grainstone),[27] the analyzed carbonate core samples are classified as Wackestone 70% and Packstone 30%. SEM analysis revealed detailed characteristics of visible porosity, including the limited interconnection between pores (Fig. 11). Additionally, the high abundance of foraminiferal tests interprets a deep-marine depositional environment for the analyzed carbonate samples.

XRD analysis revealed calcite as the dominant mineral (95.9%) in the analyzed samples, with trace amounts of dolomite and pyrite also detected (Fig. 12).

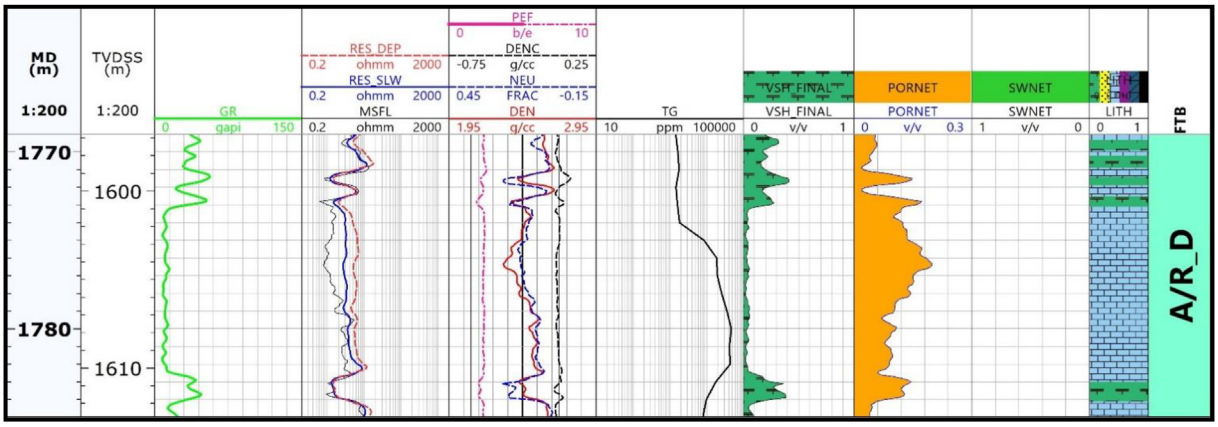

Fig. 5. Vertical distribution results of petrophysical and Lithology of AR/D reservoir in C well.

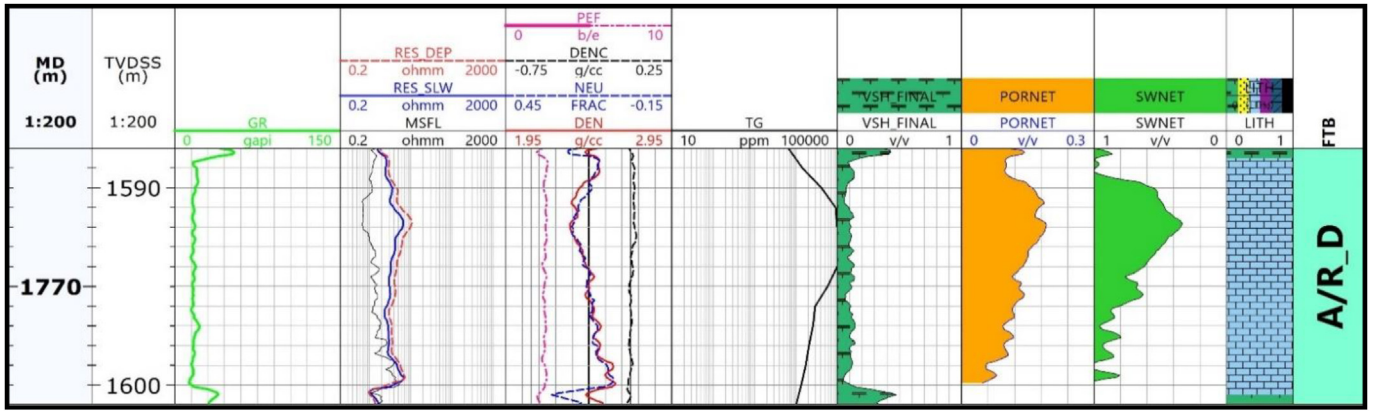

Fig. 6. Vertical distribution results of petrophysical and Lithology of AR/D reservoir in D well.

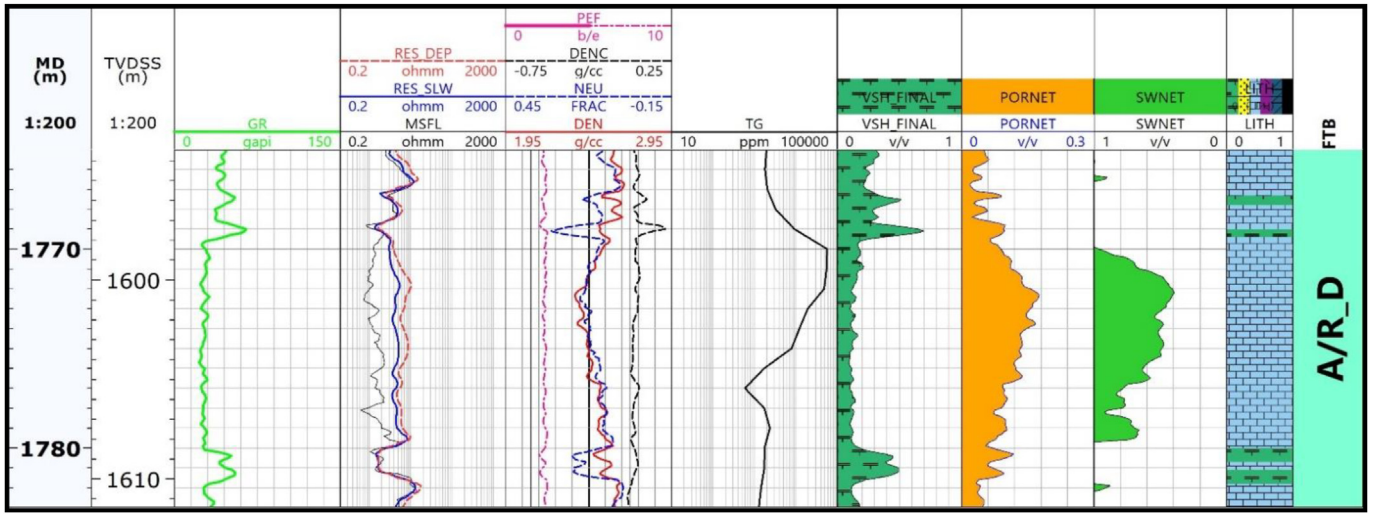

Fig. 7. Vertical distribution results of petrophysical and Lithology of AR/D reservoir in E well.

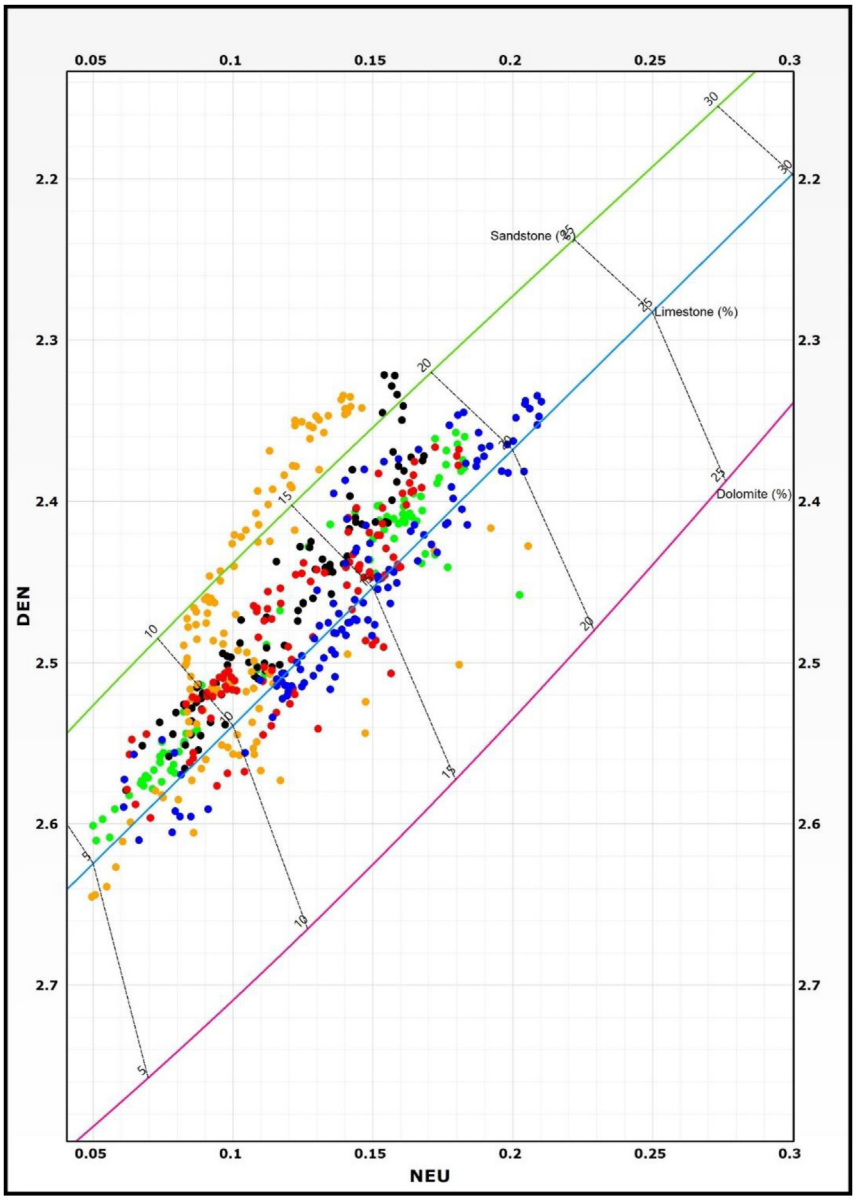

Fig. 8. Neutron-Density cross plot of all wells (A-B-C-D-E) showing the lithological components for AR/D which around the limestone line, some points around sandstone due to the gas effect as in A well.

3.4. Summary and conclusion

Exploration and development of carbonate reservoirs present greater challenges compared with their siliciclastic counterparts due to inherent complexities stemming from variations in lithology, mineralogy, pore types, connectivity, and textures. Consequently, many carbonate reservoirs either remain non-producing or are exploited at sub-commercial rates. The study revealed that the AR/D in the Petrosannan field is an attractive reservoir with limited connectivity in the petrosannan field. AR/D carbonate is predominantly composed of limestone with a net pay thickness ranging from 4.7 to 9.9 m. The reservoir porosity values range from 14 to 16% and water saturation values between 35 and 70%. The XRMI found partial open fractures in the reservoir, which may improve permeability and contribute aid hydrocarbon production. Core samples revealed a porous rock with an average porosity of 16%. XRD analysis identified calcite as the predominant mineral, accounting for 95.9% of the composition. The study suggests that implementing a stimulation program for AR/D carbonate to overcome the reservoir tightness and improve productivity and hydrocarbon recovery. A candidate well in

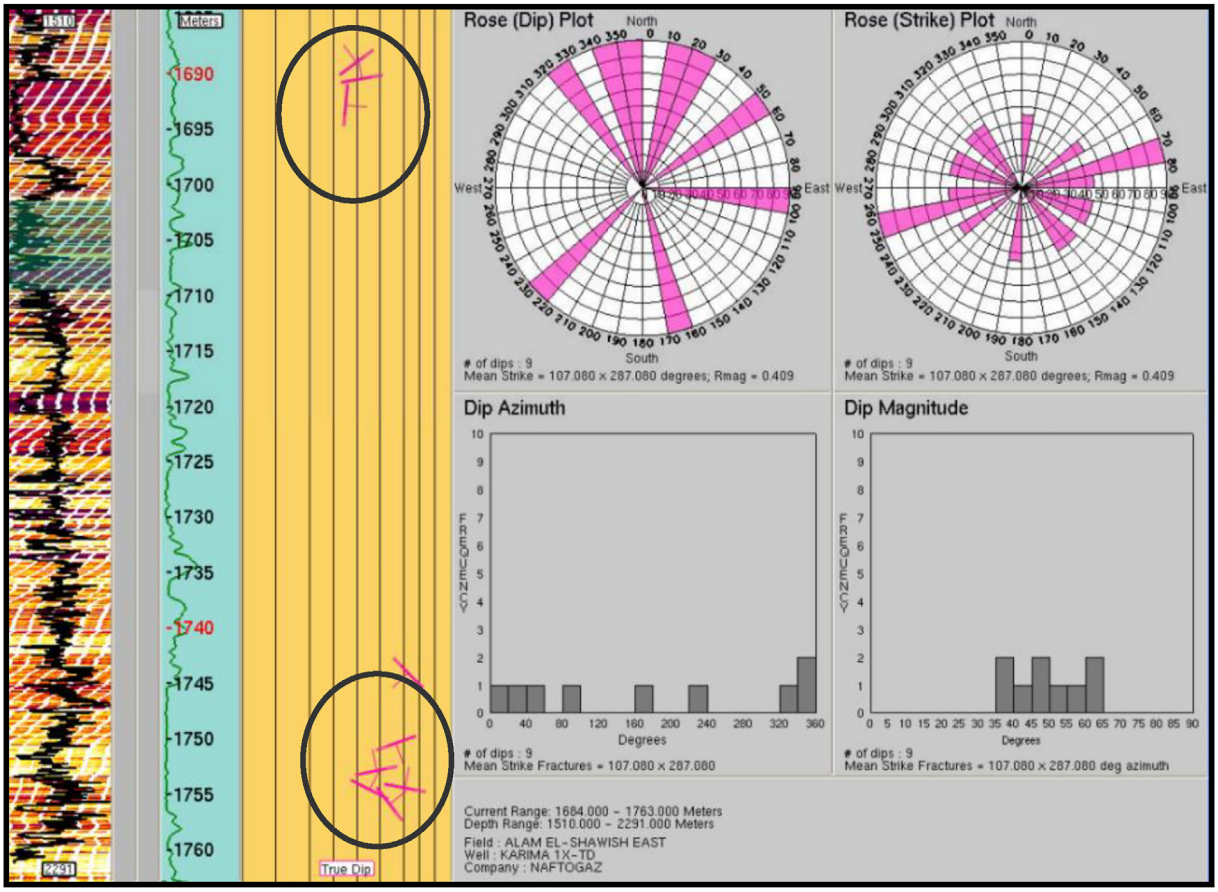

Fig. 9. Rose plots and histograms of partial open fractures with different directions around the interested zone.

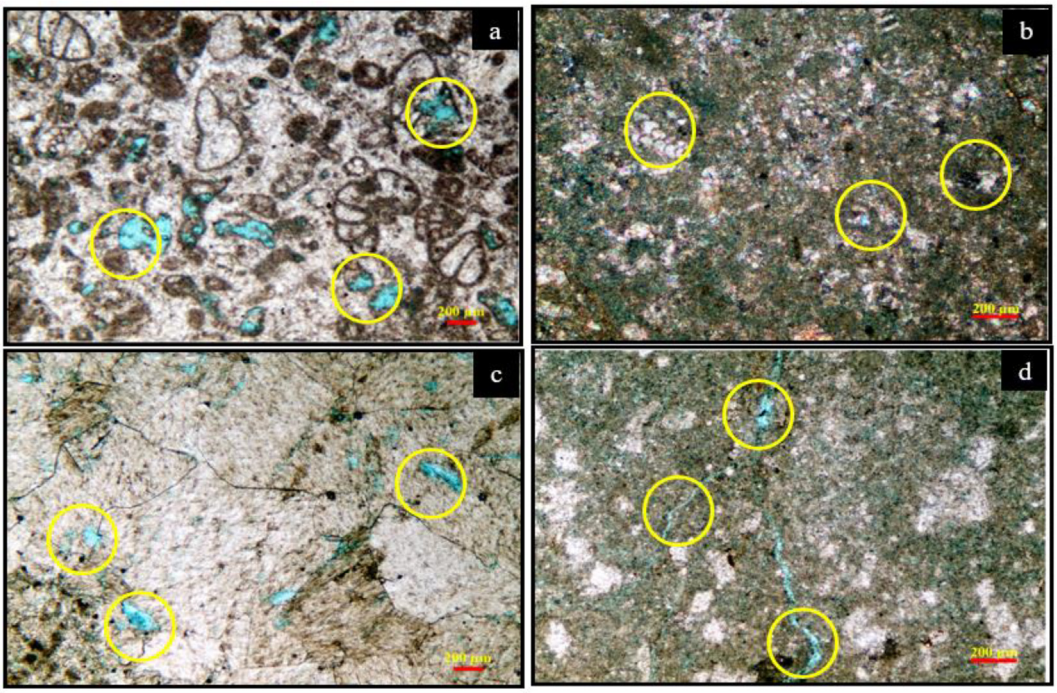

Fig. 10. (a) The bioclast types are foraminiferal tests with thin micritic envelopes. These tests exhibit variable preservation, with some filled by sparite and others partially or completely dissolved; (b) bioclasts primarily comprising foraminiferal tests with thin micritic envelopes. Some tests are filled with micro sparite. Calcite, the dominant mineral, forms a very fine micritic matrix. Trace amounts of pyrite and microcrystalline calcite and dolomite cements were also identified; (c) microcrystalline calcite and dolomite cements. Visual porosity recorded. It is about 15 % mainly of intragranular pores developed in the foraminiferal test in addition to intercrystalline porosity and (d) Calcite as the dominant mineral, forming a very fine micritic matrix. Trace amounts of pyrite were also identified. Visual porosity recorded. It is about 18 % mainly of intercrystalline in addition to channel and intragranular porosity due to dissolution.

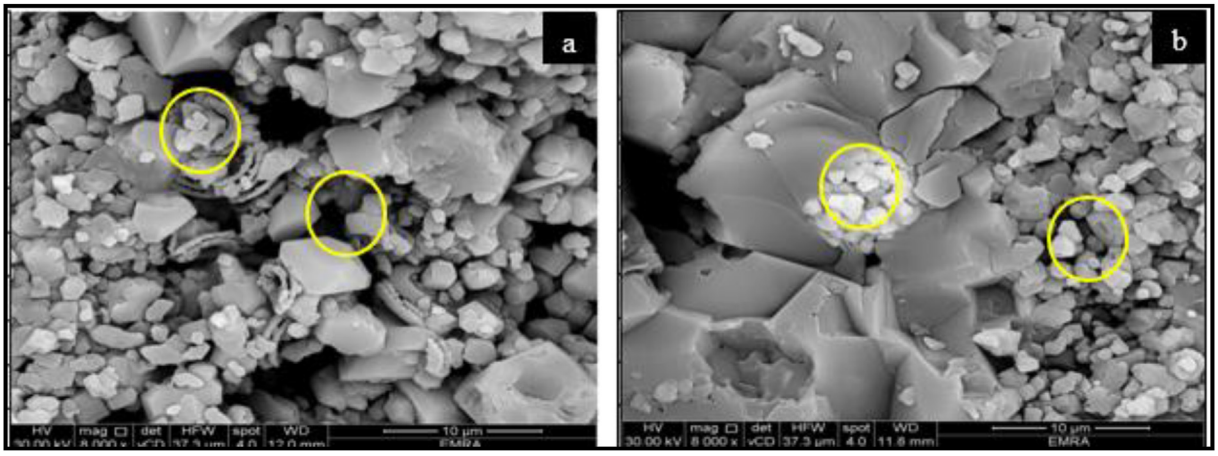

Fig. 11. (a) SEM photomicrograph showing crystalline calcite in a micritic matrix with intercrystalline porosity and traces of pyrite and (b) SEM photomicrograph showing calcite crystals and foraminiferal tests with intercrystalline porosity.

the Petrosannan field demonstrated promising performance, with an average daily oil production of ~100 barrels. The AR/D carbonate reservoirs in both the AG, notably in the Petrosannan and SWQ fields, and Gindi Basins share some key characteristics. They are primarily composed of limestone, a favorable attribute for hydrocarbon production. Additionally, the presence of fractures in both basins plays a vital role in enhancing permeability, a crucial factor for allowing fluids to flow within the reservoir. However, these seemingly similar reservoirs exhibit some significant differences in terms of net pay thickness, reservoir porosity, and water saturation net pay thickness, reservoir porosity, and water saturation between the two areas. To address these challenges and unlock the full potential of AR/D carbonate reservoirs, a two-pronged approach is recommended. Firstly, further data acquisition using advanced imaging techniques like XRMI can provide detailed insights into reservoir structure and heterogeneity. Additionally, conducting petrographic and XRD analyses of core samples can precisely characterize reservoir quality, aiding in reservoir management strategies. Secondly, reservoir stimulation programs should be implemented based on acquired data to address reservoir tightness and enhance overall productivity and hydrocarbon recovery.

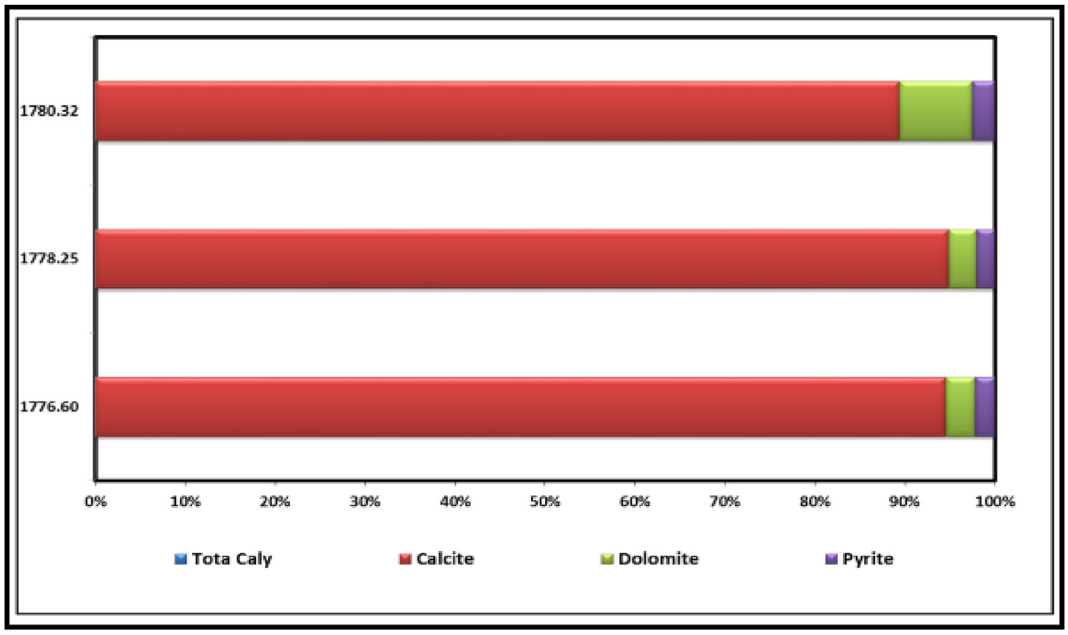

Fig. 12. Semi-quantitative radiography diffraction data of the examined samples.

Conflicts of interest

There are no conflicts of interest.

Acknowledgment

A word of gratitude is extended to the Egyptian General Petroleum Corporation (EGPC) and Petrosannan Management for their support and for providing access to the data, which allowed for the completion of this study. The authors are grateful to the anonymous reviewers for their insightful comments and suggestions, which significantly strengthened this work.

References

1. Farouk S, Sen S, Ganguli SS, et al. An integrated petrographical, petrophysical and organic geochemical characterization of the Lower Turonian Abu Roash-F carbonates, Abu Gharadig field, Egypt – Inferences on self-sourced unconventional reservoir potential. *Mar Petrol Geol*. 2022;145:105885.
2. Sarhan MA, Selim ES. Geophysical appraisal of fractured carbonate reservoirs: a case study of Abu Roash D member, Abu Gharadig field, Western Desert, Egypt. *Euro-Mediterr J Environ Integr*. 2023;8:395–408.
3. Robertson Research I, Associated Resource Consultants I, Scott P, Associates ERCER. *Consultants, and l.-B. L. Muʾassasah Al-Miṣrīyah Al-ʿĀmmah, Petroleum Potential Evaluation, Western Desert, the Arab Republic of Egypt, p.ˆpp. 8 Volumes : Illustrations ; 29 Cm, Gwynedd, Wales. Gwynedd*. Wales: Robertson Research International Ltd; 1982.
4. E. G. P. *Corporation, Western Desert, Oil and Gas Fields: (A Comprehensive Overview)*. Egyptian General Petroleum Corporation; 1992.
5. Moustafa A. *Mesozoic-Cenozoic Basin Evolution in the Northern Western Desert of Egypt*. vol. 3. The Geology of East Libya; 2008: 29–46.
6. Abdel Aal A, Moustafa A. *Structure framework of the Abu Gharadig basin, Western Desert, Egypt, 9 EGPC Expl. and Prod. in Conf. Cairo*. 1988.
7. Hamimi Z, El-Barkooky A, Frías JM, Fritz H, Abd El-Rahman Y. *The Geology of Egypt*. New York, USA: Springer; 2020.
8. Meshref W, Abu El Karamat M, El Gindi M. Exploration concepts for oil in the Gulf of Suez. In: *9th Petroleum Exploration and Production Conference, Cairo*. 1988.
9. Kargarpour MA. Carbonate reservoir characterization: an integrated approach. *J Pet Explor Prod Technol*. 2020;10:2655–2667.
10. Fitch PJR. *Heterogeneity in the Petrophysical Properties of Carbonate Reservoirs*. University of Leicester; 2011.
11. Zoveidavianpoor M, Samsuri A, Reza S. Well stimulation in carbonate reservoirs: the needs and superiority of hydraulic fracturing. *Energy Sources Part A Recovery Util Environ Eff*. 2013; 35:92–98.
12. Gidley JL. *Recent Advances in Hydraulic Fracturing*. 1989.
13. Schlumberger A. *A Guide to Well Site Interpretation of the Gulf Coast*. Houston: Schlumberger Well Services; 1975.
14. Asquith GB, Gibosn CR. *Basic Well Log Analysis for Geologists*. Tulsa, USA: American Association of Petroleum Geologists; 1982.
15. Nouh AZ. The relation between the shale origin (source or non source) and its type for Abu Roash formation at wadi El-Natrun area, south of Western Desert, Egypt. *Aus J Basic Appl Sci*. 2008;2:360.
16. Atlas D. *Log Interpretation Charts*. 1985.
17. Islam A, Islam MA, Tasnuva A, Biswas RK, Jahan K. Petro physical parameter studies for characterization of gas reservoir of Norshingdi gas field, Bangladesh. *Int J Adv Geosci*. 2014; 2:53–58.
18. Bateman R, Konen C. The log analyst and the programmable pocket calculator. *Log Analyst*. 1978;19:4.
19. Schlumberger. *Cased Hole Log Interpretation: Principles/applications*. Schlumberger Educational Services; 1989.
20. Archie GE. The electrical resistivity log as an aid in determining some reservoir characteristics. *Transact AIME*. 1942; 146:54–62.
21. Serra O. *Well Logging and Reservoir Evaluation*. 2007 (No Title).
22. Ekstrom MP, Dahan CA, Chen MY, Lloyd PM, Rossi DJ. Formation Imaging with Microelectrical Scanning Arrays. In: *SPWLA 27th Annual Logging Symposium*. 1986.
23. Victor RA, Prodanović M, Torres-Verdín C. Monte Carlo approach for estimating density and atomic number from dual-energy computed tomography images of carbonate rocks. *J Geophys Res Solid Earth*. 2017;122:9804–9824.
24. Nabway BS, Kassab MA. Porosity-reducing and porosity-enhancing diagenetic factors for some carbonate microfacies: a guide for petrophysical facies discrimination. *Arabian J Geosciences*. 2014;7:4523–4539.
25. Gomaa MM, Kassab MA, El-Sayed NA. Study of pertrographical and electrical properties of some Jurassic carbonate rocks, north Sinai, Egypt. *Egypt J Petrol*. 2015;24:343–352.
26. Tavakoli V. *Carbonate Reservoir Heterogeneity: Overcoming the Challenges*. New York, USA: Springer Nature; 2019.
27. Dunham RJ, Ham WE. *Classification of carbonate rocks According to depositional Texture1, Classification of Carbonate Rocks—A Symposium*. Tulsa, USA: American Association of Petroleum Geologists; 1962, 0.
28. Aljuboori FA, Lee JH, Elraies KA, Stephen KD. Gravity drainage mechanism in naturally fractured carbonate reservoirs; review and application. *Energies*. 2019;12:3699.